

A Mechanistic Study on the Effect of Salt Concentration on Uniform Corrosion Rate of Pipeline Steel in Acidic Aqueous Environments

Fazlollah Madani Sani, Bruce Brown, Srdjan Nestic
Institute for Corrosion and Multiphase Technology, Ohio University
342 W State Street
Athens, Ohio, 45701
USA

ABSTRACT

CO₂/H₂S corrosion in oil and gas fields is often associated with acidity and salinity of fluids. However, the role of salinity is usually ignored in corrosion studies and corrosion prediction models. As part of a major project to model uniform CO₂/H₂S corrosion of carbon steel oil and gas pipelines in high salinity environments, the research reported herein investigated uniform CO₂ corrosion in high salinity acidic media. Experiments were carried out using a rotating disk electrode (RDE) in CO₂-saturated aqueous solutions at 10°C and a constant pH of 3.0, whilst varying NaCl concentration from 1 wt.% to 20 wt.%. The RDE setup was used because mass transfer of species to the surface in this setup is well understood. A low temperature was chosen to better distinguish between charge transfer and mass transfer-controlled reactions underlying the corrosion process. Surface analysis indicated that the corrosion process was uniform, and no corrosion layer formed on the steel surface. Both linear polarization resistance (LPR) and potentiodynamic polarization (PD) techniques showed a general decrease in the uniform corrosion rate with increasing salt concentration. The analysis of the PD sweeps showed that salt concentration did not influence the mechanism of anodic and cathodic reactions and the decrease in the corrosion rate was due to deceleration in the rate of both anodic and cathodic reactions. Modeling results showed that salt concentration mostly affected the rate of mass transfer of H⁺ ion to the surface by changing H⁺ diffusion coefficient and H⁺ activity coefficient.

Keywords: Uniform CO₂ corrosion, salt concentration, salinity, non-ideal solutions, rotating disk electrode (RDE), produced water

INTRODUCTION

Dissolved salts are generally present in water produced during hydrocarbon production from underground reservoirs.¹ It is reported that, in the USA, the concentration of salts (i.e. salinity) in water produced from conventional hydrocarbon reservoirs can vary from 1000 mg/l (~0.1 wt.%) to 400,000 mg/l (~28 wt.%).² In addition to salts, dissolved corrosive gases (CO₂ and H₂S) are present in produced water, which make the mixture a complex corrosive environment for metallic parts and equipment used throughout the production process.

Internal CO₂ corrosion of carbon steel tubulars is a common type of corrosion that occurs in the oil and gas industry.³ A large body of research exists on CO₂ corrosion. However, most of this research has been focused on low salt concentrations ranging from 1 to 3 wt.%, which is often much lower than what is usually encountered in the field.⁴ There are few studies on uniform CO₂ corrosion at salt concentrations above 3 wt.%. In recent comprehensive work reported by Madani Sani *et al.*⁵ the uniform CO₂ corrosion rate of carbon steel reached a maximum between 1 wt.% to 3 wt.% NaCl and then decreased continuously by further increase in NaCl concentration. The decrease in the corrosion rate was attributed to the retardation of both anodic and cathodic reactions. Similar results have been published by Eliyan, *et al.*^{6,7}, and Liu, *et al.*⁸ However, Fang³, Zeng, *et al.*⁹, and Han, *et al.*¹⁰ who reported a continuous declining trend in the rate of uniform CO₂ corrosion of carbon steel with increasing NaCl concentration.

This work, as a small part of a large ongoing joint-industrial project (JIP) focused on corrosion mechanisms related to the internal CO₂/H₂S corrosion of pipeline-grade carbon steel, covers the effect of salt concentration on uniform CO₂ corrosion in acidic media. The data presented in this article will be used in development of a corrosion-rate-prediction model as one of the final goals of the JIP.

In this paper, the effect of NaCl concentration on corrosion behavior of X65 carbon steel was investigated by performing electrochemical experiments in CO₂-saturated aqueous solutions with different NaCl concentrations (1 wt.% to 20 wt.%) at 10°C, 1 bar total pressure and pH 3.

EXPERIMENTAL PROCEDURE

Setup and apparatus

Figure 1 shows the experimental apparatus. Experiments were carried out in a custom-made glass cell with an outer jacket for temperature control. An industrial chiller (not visible in Figure 1) was used to circulate glycol (the green liquid in Figure 1) through the outer jacket for controlling the solution temperature during the experiments. Glycol did not have any contact with the experimental solution.

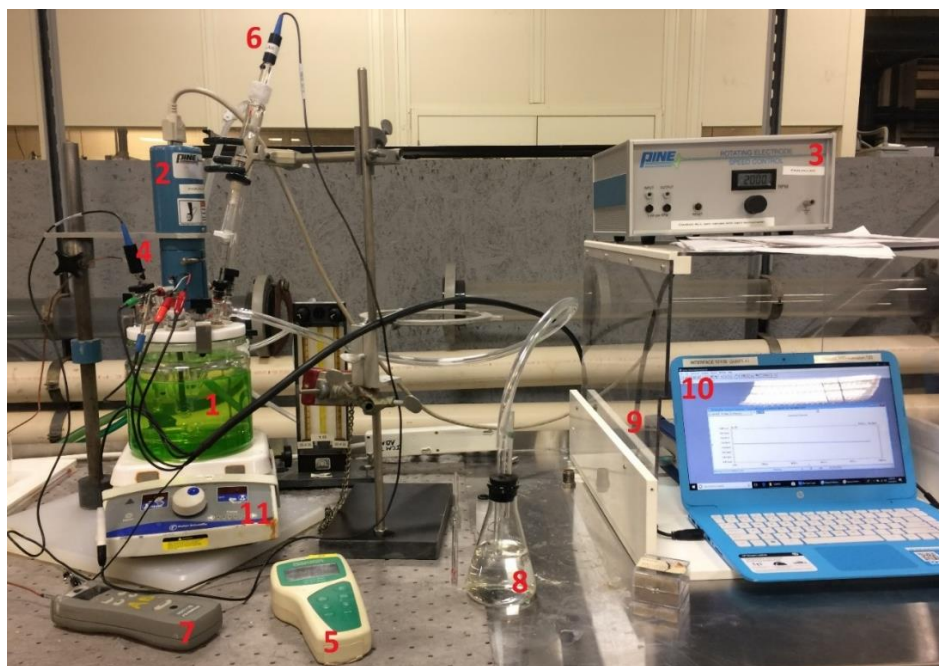


Figure 1. The experimental apparatus: (1) glass cell, (2) motor, (3) rotation speed controller, (4) pH probe, (5) pH meter, (6) Ag/AgCl reference electrode, (7) thermometer, (8) gas out bubbler, (9) potentiostat for data acquisition, (10) laptop for data collection, (11) hot plate stirrer.

Figure 2 shows a close-up view of the glass cell. A conventional three-electrode setup was used for the experiments that included a rotating disk electrode (RDE) assembly as the working electrode, a graphite bar as the counter electrode and an Ag/AgCl electrode as the reference electrode. The counter electrode was mounted in a glass tube with a porous tip to avoid interference of species (such as H₂ and O₂) that form on the counter electrode during the potential sweep, with the corrosion process. The porous tip provides ionic conductivity between the counter electrode and the solution. The reference electrode was placed in a Luggin capillary that was filled with 1M KCl. The capillary tip was adjusted close to the RDE almost at the same level to diminish the effect of solution resistance on the electrochemical measurements, but, not too close to disturb the RDE laminar flow (approximately 3 mm from the Teflon RDE holder). The immersion depth for the RDE was in the middle of the glass cell. However, it is reported that the RDE immersion depth does not influence the electrochemical measurements.¹¹



Figure 2. A picture of the custom-made glass cell and its components used in the RDE electrochemical experiments: (1) glass cell, (2) outer jacket, (3) Teflon lid, (4) clamp, (5) coolant (glycol) in, (6) coolant out, (7) RDE and its holder, (8) pH probe, (9) Luggin capillary for the Ref. electrode, (10) counter electrode, (11) thermocouple, and (12) magnetic stirring bar.

RDE Specimen

The RDE specimen was a carbon steel cylinder with a diameter of 5 mm and a height of 4 mm. The specimen was flush mounted in a Teflon holder as shown in Figure 3. The assembly was polished before each experiment. The two red O-rings were used to seal the connection between the specimen holder and the RDE shaft.



Figure 3. (a) The bottom view of the RDE specimen flush mounted in a Teflon holder, (b) The side view of the specimen holder.

Material

The carbon steel grade used for the experiments was API 5L X65, a common steel grade for oil and gas transmission pipelines.¹² Table 1 shows the chemical composition of the experimental steel. The carbon steel microstructure (not shown here) was uniform, fine structure of pearlite in a ferrite matrix.

Table 1: Chemical composition of the experimental carbon steel (API 5L X65) (in wt.%).

Al	As	C	Co	Cr	Cu	Mn	Mo	Nb	Ni
0.028	0.008	0.05	<0.001	0.252	0.173	1.51	0.092	0.034	0.291
P	S	Sb	Si	Sn	Ti	V	Zr	Fe	
0.004	<0.001	<0.001	0.167	0.002	0.012	0.04	<0.001	balance	

Electrochemical measurements

Experiments were conducted in CO₂-saturated aqueous solutions with different NaCl concentrations to investigate the effect of salt concentration on uniform CO₂ corrosion. NaCl is the major salt present in water produced from conventional hydrocarbon reservoirs;¹³ thereby, it was chosen for the present study. A low solution temperature of 10°C was chosen for the experiments. Lower temperatures slow down the kinetics of the electrochemical reactions at the metal surface more than the rate of diffusion of electroactive species to the metal surface. This results in more separation between the charge transfer and the mass transfer-controlled regions of the cathodic potentiodynamic sweeps and facilitates evaluation of the effect of salt concentration on each region. Even though it has been shown that corrosion due to the presence of 1 bar CO₂ is not dominant at pH lower than 4¹⁴, experiments were conducted in an acidic medium of pH 3 to broaden the range of data required for developing a CO₂ corrosion prediction model at high ionic strength.

For each experiment, NaCl was dissolved in one liter of deionized water (18 MΩ.cm) in the glass cell. The solution was then sparged with CO₂ for at least 2 h, while being stirred. After about 1 h of sparging, pH of solution reached to a stable value (Table 2). At this point, pH was adjusted to 3.0 by adding 0.1 M HCl to the solution. More HCl was required for low NaCl concentrations. The specimen assembly (shown in Figure 3) was sequentially wet polished with 240-, 400- and 600-grit abrasive papers. Subsequently, the assembly was ultrasonically degreased with isopropanol for 3 min and dried in cool N₂ gas prior to immersion in the test solution.

Table 2. The autogenous pH of CO₂-saturated aqueous solutions for different NaCl concentrations at 10°C and 1 bar total pressure.

NaCl concentration (wt.%)	1	3	10	20
Avg. autogenous pH	3.83	3.75	3.61	3.45

After introducing the RDE assembly to the solution and prior to each electrochemical test, the open circuit potential (OCP) was monitored until a stable potential value ($\Delta E_{OCP} < 2$ mV/min) was achieved. The linear polarization resistance (LPR) technique was performed to measure the corrosion rate. Electrochemical impedance spectroscopy (EIS) was carried out to determine the solution resistance (iR drop). Potentiodynamic polarization (PD) was done to study the effect of salt concentration on the mechanism of uniform CO₂ corrosion. A Gamry Reference 600[†] potentiostat was used for all the electrochemical measurements. Table 3 and Table 4 summarize the conditions and the methods used in the experiments. Each test was repeated two times in order to check the reproducibility of results.

[†] Trade name

Table 3. The experimental conditions for studying the effect of salt concentration on uniform CO₂ corrosion of carbon steel.

Parameter	Description
Specimen material	X65 carbon steel
RDE diameter (mm)	5.00 ± 0.05
Temperature (°C)	10.0 ± 0.5
Total pressure (bar)	1
CO ₂ partial pressure (bar)	0.97
NaCl concentration (wt.%)	1, 3, 10 and 20
pH	3.00 ± 0.02
RDE rotational speed (rpm)	2000 ± 2

Table 4. The experimental methods for studying the effect of salt concentration on uniform CO₂ corrosion of carbon steel.

Method	Description
Potentiodynamic polarization <ul style="list-style-type: none"> • Potential range (V vs. OCP) • Scan rate (mV/s) 	-1.0 to 0.2 0.5
Linear polarization resistance <ul style="list-style-type: none"> • Potential range (mV vs. OCP) • Scan rate (mV/s) 	-5.0 to 5.0 0.125
Electrochemical impedance spectroscopy <ul style="list-style-type: none"> • Frequency range (Hz) • DC voltage (V vs. OCP) • Peak to peak amplitude (mV) • Sampling rate (points/decade) 	10,000 to 0.1 Zero 10 8

Experimental considerations

1. The level of dissolved oxygen, monitored by an Orbisphere[†] 410 oxygen meter at the gas outlet, was kept less than 10 ppb during the experiments.
2. Temperature could not be kept constant by just circulating coolant in the glass cell jacket. Therefore, a hot plate was used continuously to balance the temperature. A constant temperature of 10 ± 0.5°C was achieved by an equilibrium between coolant circulation and the hot plate.
3. Measuring pH correctly in solutions with high salinity is challenging.¹⁵ The pH measurements were done with a double-junction pH probe, which was resistant to Na⁺ ion interference.
4. At low NaCl concentrations, H₂ gas bubbles formed on the surface of the RDE in the cathodic potentials and caused spikes in the PD sweeps as seen in Figure 5.
5. Since there was no significant difference in the PD sweeps for scan rates of 0.125 mV/s and 0.5 mV/s, the latter was chosen for PD experiments.
6. Figure 4 compares the cathodic sweeps at the two scan rates for 20 wt.% NaCl.

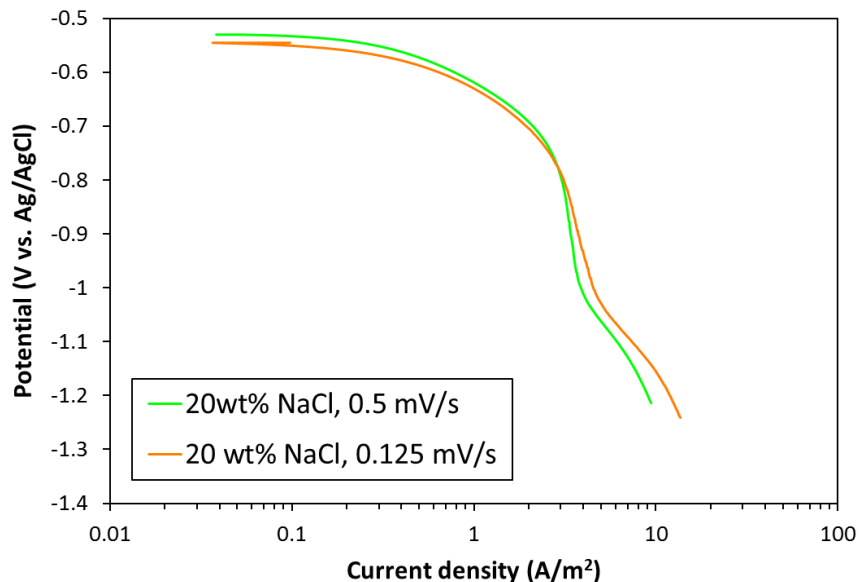


Figure 4. The cathodic sweeps for X65 carbon steel RDE specimen obtained at two scan rates of 0.125 and 0.5 mV/s in 20 wt.% NaCl aqueous solution at 1 bar CO₂, 10°C, and pH 3.

RESULTS AND DISCUSSION

Potentiodynamic polarization sweeps

The main electrochemical reactions underlying aqueous CO₂ corrosion of mild steel are active dissolution of iron:



and reduction of hydrogen ions:



Figure 5 shows the PD sweeps at different NaCl concentrations. The potential values are corrected for the solution resistance (*iR* drop) in all the sweeps. At least, two sets of PD sweeps were obtained for each NaCl concentration to verify the reproducibility of results. Increasing NaCl concentration altered both anodic and cathodic branches. For a precise analysis of the effect of NaCl concentration on the CO₂ corrosion process, Tafel analysis was used to extract the electrochemical features of the PD sweeps.¹⁴ The fitted sweeps for two NaCl concentrations are shown in Figure 6 as a demonstration of fitting exercise accuracy. The Tafel analysis results are listed in Table 5. The electron transfer coefficient for H⁺ reduction reaction (α_{H^+}) deviated slightly from the theoretical value of 0.5, commonly considered for the hydrogen evolution on an iron surface.¹⁶ Similar deviations have been reported in the literature.^{17,18} The Tafel slope ($\beta=2.3RT/\alpha F$) for H⁺ reduction reaction changed marginally with increasing NaCl concentration. This implies that NaCl concentration did not influence the mechanism of cathodic H⁺ reduction reaction. The electron transfer coefficient for active anodic dissolution of iron (α_{Fe}) was 1.10 for all NaCl concentrations. Bockris *et al.*¹⁶ proposed 1.5 for iron dissolution in acidic media without the presence of halides. Chin and Nobe¹⁹ reported 1.18 for dissolution of iron in acidic chloride media, which is very close to the results of this study. Since α_{Fe} (i.e., the anodic Tafel slope) did not change with increasing NaCl concentration, it can be concluded that the mechanism of anodic dissolution of iron in the active region remained unchanged. The mechanisms of iron dissolution in the presence of chloride has been comprehensively explained elsewhere.^{5,20–22}

The reference current densities for both H^+ reduction (i_{0,H^+}^{ref}) and iron dissolution ($i_{0,Fe}^{ref}$) reactions decreased with the addition of NaCl concentration. The reference current densities are arbitrary current densities used to draw the cathodic and anodic Tafel lines and find the best fits to the PD sweeps. The Magnitude of reference current densities indicates the rate of charge transfer controlled cathodic and anodic reactions. Thus, increasing NaCl concentration decreased the rate of both cathodic and anodic charge transfer reactions. The decrease in the rate of cathodic reaction may be attributed to the coverage of electrochemically active sites on the steel surface by chloride ions.^{5,20-22} The decrease in the anodic reaction rate can be explained by the decrease in the activity of OH^- ion as a result of the increase in NaCl concentration ($i_{ct,Fe} \sim a_{OH^-}^x$). By using the Tafel analysis data and a water chemistry model based on Li and Duan publication²³, the anodic reaction order with respect to OH^- ion, x , was found to be approximately 1. However, no significant dependency was found between the anodic reaction rate and the activity of chloride ion ($i_{ct,Fe} \sim a_{Cl^-}^y$), i.e., the anodic reaction order with respect to Cl^- ion, y , was close to zero. Using the same practice as that for OH^- , y was obtained to be approximately 0.1.

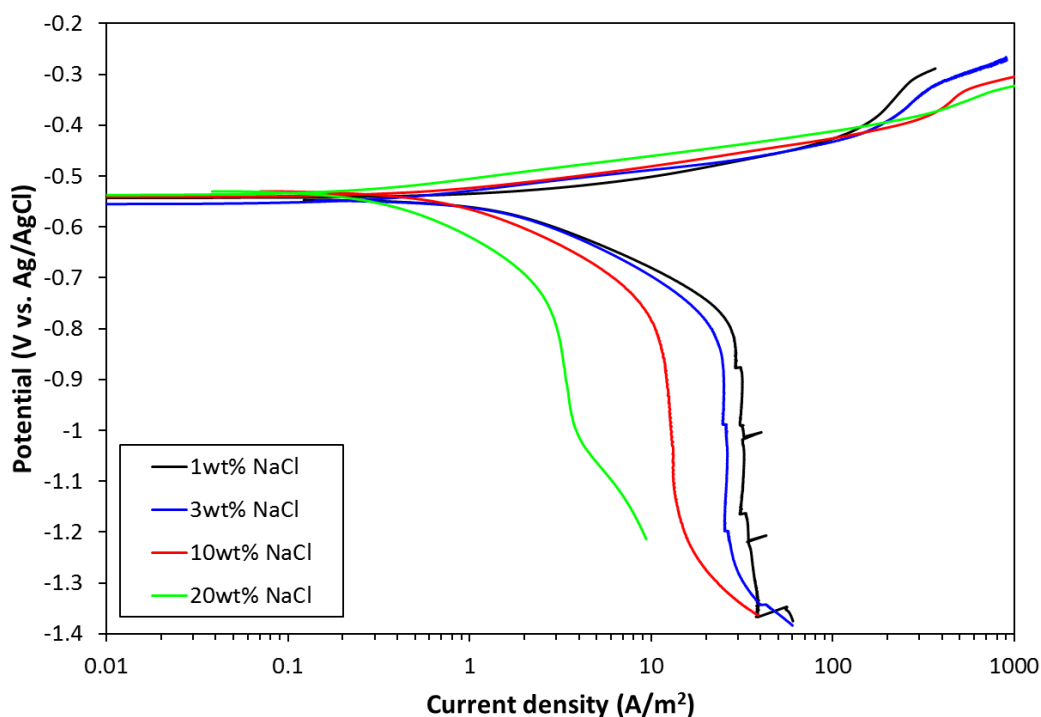


Figure 5. Potentiodynamic polarization sweeps in CO_2 -saturated solutions with different NaCl concentrations at $10^\circ C$, 1 bar total pressure, pH 3, and 2000 rpm RDE rotational speed.

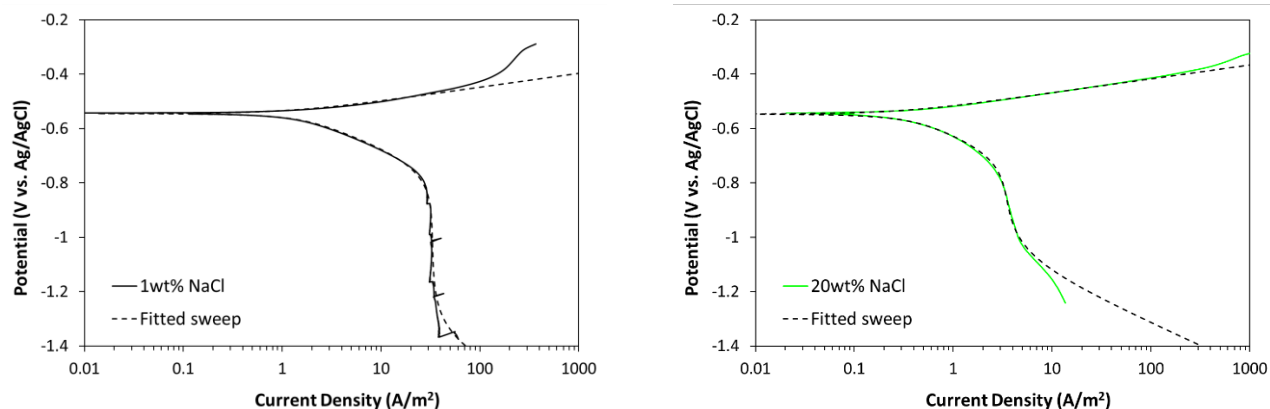


Figure 6. Fitted sweeps obtained by Tafel analysis for two NaCl concentrations

Table 5. The average electron transfer coefficients (α), Tafel slopes (β) and reference exchange current densities (i_0^{ref}) for H⁺ reduction, Fe dissolution, and H₂O reduction reactions; and the corresponding B values* obtained by fitting the PD sweeps with Tafel lines.¹⁴

NaCl concentration (wt.%)	α_{H^+}	α_{Fe}	β_{H^+}	β_{Fe}	B value	β_{H_2O}	i_{0,H^+}^{ref}	$i_{0,Fe}^{ref}$	i_{0,H_2O}^{ref}
							mV/dec		
1	0.44	1.10	128	51	15.8	0.75 β_{H^+}	0.08	4.0e-3	N/A
3	0.43	1.10	129	51	15.9		0.08	3.5e-3	5.0e-5
10	0.43	1.10	131	51	15.9		0.06	1.3e-3	1.2e-4
20	0.45	1.10	125	51	15.7		0.03	9.0e-4	3.1e-4

Modeling cathodic limiting current density

The key change in the PD sweeps with the addition of NaCl concentration was the decrease in the cathodic limiting current density (i_L). i_L which represents the rate of mass transfer of electroactive species to the metal surface, depends on concentration and diffusivity of electroactive species in the bulk solution, density and viscosity of solution. For an RDE operating under laminar flow regime (Reynolds number < 1.7×10⁵)¹¹, i_L in A/m² can be determined using Levich's equation:

$$i_L = 6200 \times n \times F \times \omega^{0.5} \times \rho^{1/6} \times \mu^{-1/6} \times D^{2/3} \times C_b \quad (3)$$

where, n is the number of electrons involved in the electrode reaction; F is the Faraday constant (96485 C/mol); ω is the RDE angular velocity (rad/s); ρ is the density of the solution (g/cm³); μ is the dynamic viscosity of the solution (g/cm-s); D is the diffusion coefficient of electroactive species (cm²/s); and C_b is concentration of electroactive species in the bulk solution (mol/cm³).

Figure 7 compares the experimental limiting current density (squares) with that calculated from Equation (3) (solid line) at different NaCl concentrations. At pH 3, the contribution of buffering effect (H⁺ ions produced by dissociation of H₂CO₃) in total i_L is negligible. For example, under the experimental conditions, $i_{L,H_2CO_3} \cong 0.04 i_L$ at 1 wt.% NaCl and $i_{L,H_2CO_3} \cong 0.02 i_L$ at 20 wt.% NaCl. Therefore, only H⁺ reduction was considered in i_L calculations.

The “pure water” line in Figure 7 indicates i_L when density, viscosity, H⁺ diffusion coefficient and H⁺ concentration in Eq. 1 are those for pure water (i.e., at zero wt.% NaCl). The other lines are calculated as discrete improvement steps:

- “Rho”: only density of solution changes with NaCl concentration and the other three parameters are those for pure water.
- “Rho+Mu”: density and viscosity of solution change with NaCl concentration and the other two parameters are those for pure water.
- “Rho+Mu+D”: density and viscosity of solution and diffusion coefficient of H⁺ change with NaCl concentration and H⁺ concentration is that for pure water.
- “Rho+Mu+D+[H⁺]”: the effect of NaCl concentration is considered in relation to all four parameters.

According to Figure 7, the variations in i_L with NaCl concentration are minor when only changes in density and viscosity of the solution are considered. However, i_L varies substantially when the effects of NaCl concentration on H⁺ diffusion coefficient and H⁺ concentration (water chemistry) are accounted for in the calculations. This means that NaCl concentration mostly affects i_L by changing the diffusion coefficient of H⁺ ion and speciation equilibria.

* The B value used in Stern-Geary equation ($B = \frac{\beta_c \times \beta_a}{2.3(\beta_c + \beta_a)}$)

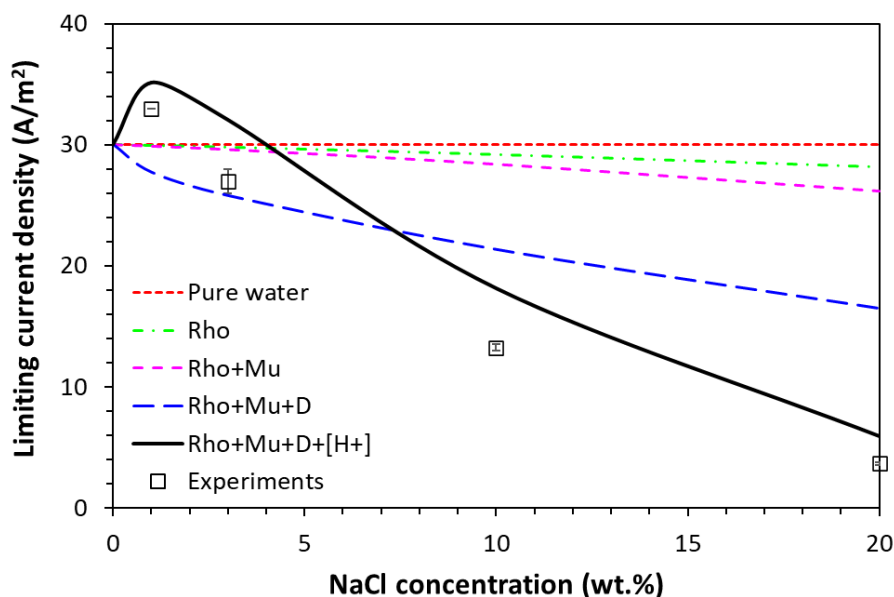


Figure 7. The cumulative changes in H⁺ limiting current density calculated with Levich's equation when the effect of NaCl concentration is applied to solution density (Rho), solution viscosity (Mu), H⁺ diffusion coefficient (D) and H⁺ concentration ([H⁺]).

The trend observed for i_L with respect to NaCl concentration in Figure 7 is similar to that for H⁺ concentration. Figure 8 depicts concentration, activity coefficient, and activity of H⁺ ion in the solution vs. NaCl concentration, calculated via the Li and Duan water chemistry model²⁴. When NaCl concentration was increased from 0 wt.% to 20 wt.%, H⁺ concentration first increased and then decreased, while the activity coefficient of H⁺ behaved in an opposite manner. However, the product of these two, *i.e.*, activity, remained constant, which agrees with the constant experimental pH. The observed trend for H⁺ concentration with respect to NaCl concentration can be attributed to changes in ionic interactions between dissolved species that altered the activity coefficients, and thereby the dissociation equilibria.

5,25

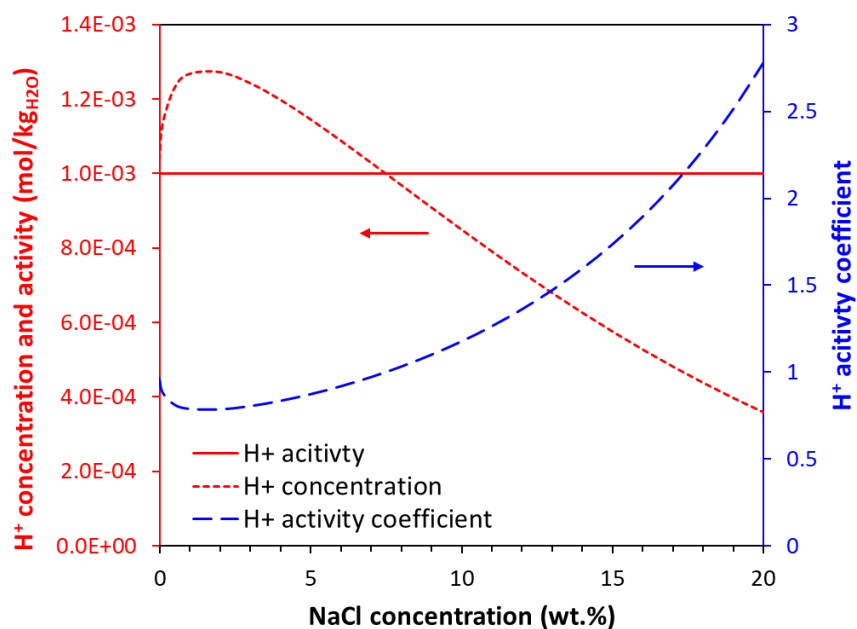


Figure 8. Calculated H⁺ activity, concentration and activity coefficient vs. NaCl concentration at 10°C, 1 bar total pressure and pH 3.

The difference between the calculated (solid line) and the experimental i_L shown in Figure 7 might be because of inaccuracies in the water chemistry model and/or H^+ diffusion coefficient equation. This requires further investigation; however, it is not the focus of this study.

Surface analysis

Figure 9 shows SEM/EDX[†] results for a freshly polished steel surface and the corroded steel surface in 1 and 20 wt.% NaCl solutions. The morphology of the corroded surface was similar for both NaCl concentrations. The EDX elemental analysis of the steel surface detected a similar composition for all three cases, which means that no corrosion layer formed on the surface when carbon steel specimens exposed to the experimental solution. Oxygen in the EDX spectrum for 1 wt.% NaCl was most likely due to the exposure of the specimen to air prior to conducting the EDX analysis.

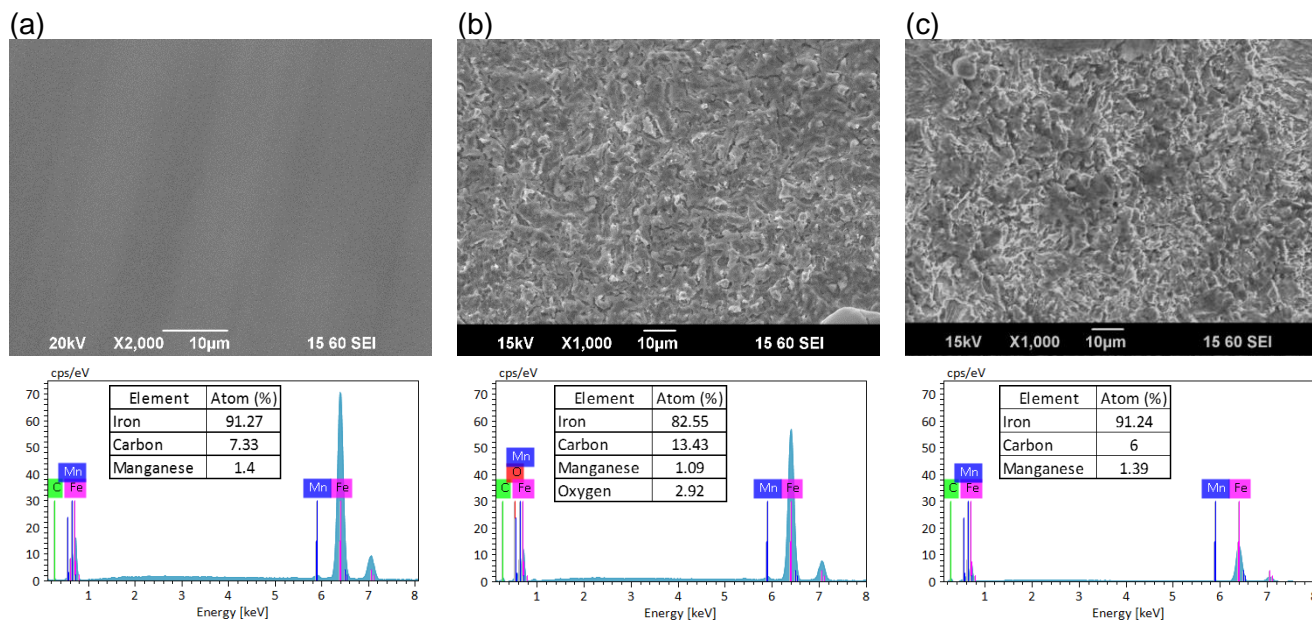


Figure 9. SEM/EDX results for (a) freshly polished steel surface, (b) corroded surface in 1 wt.% NaCl solution and (c) corroded surface in 20 wt.% NaCl solution.

Figure 10 shows the surface profilometry of the corroded steel specimens in 1 and 20 wt.% NaCl solutions obtained with an Alicona[‡] optical profilometer. The 1D profiles show changes in the surface roughness along the vertical red lines drawn on the 2D profiles. No indication of localized corrosion was detected over the entire surface of the corroded steel specimens from tests in both solutions. Therefore, it can be concluded that the specimens were corroded uniformly in both NaCl solutions under the experimental conditions. Surface analysis indicated that carbon steel surface was corroded uniformly, and no corrosion layer formed on the steel surface under the experimental conditions.

[†] Scanning electron microscopy coupled with energy dispersive spectroscopy

[‡] Trade name

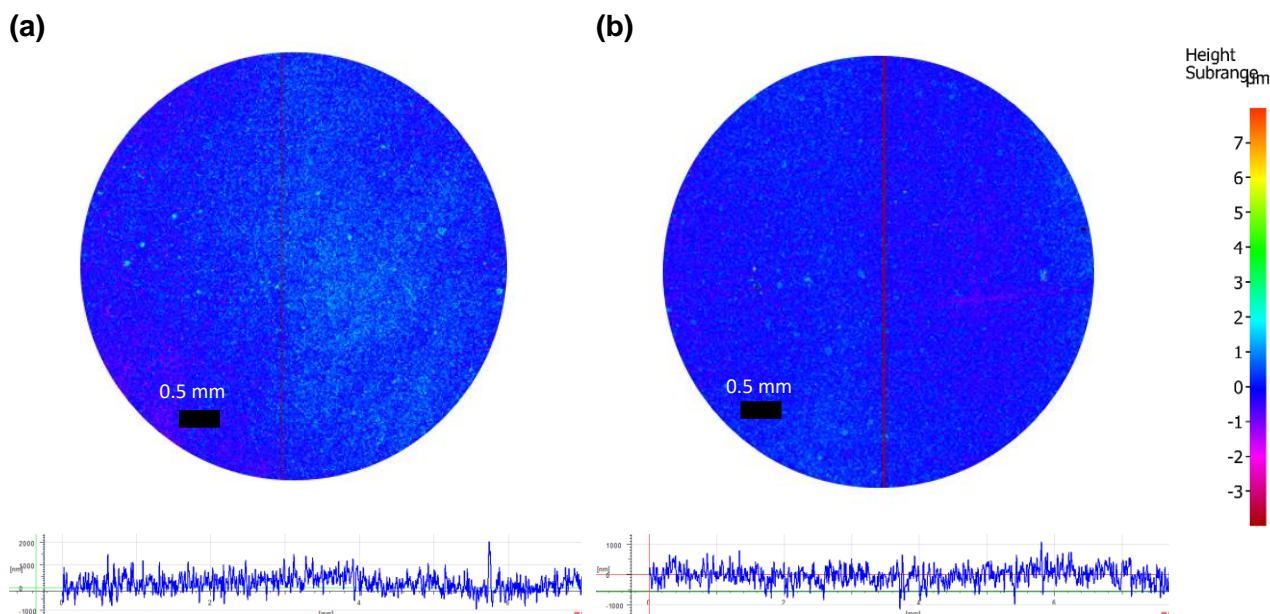


Figure 10. 2D (above) and 1D (below) surface profilometry of the corroded steel surface in 1 wt.% (a) and (b) 20 wt.% NaCl solutions.

Corrosion rate measurements

Figure 11 shows the RDE corrosion rate obtained from LPR measurements and PD sweeps at different NaCl concentrations. The B values listed in Table 5 were used for converting the measured polarization resistance (R_p) to the corrosion rate. The PD corrosion rate was extracted from the sweeps by Tafel analysis. A similar trend and a similar magnitude of corrosion rates were obtained with both techniques, showing that the results were reliable.

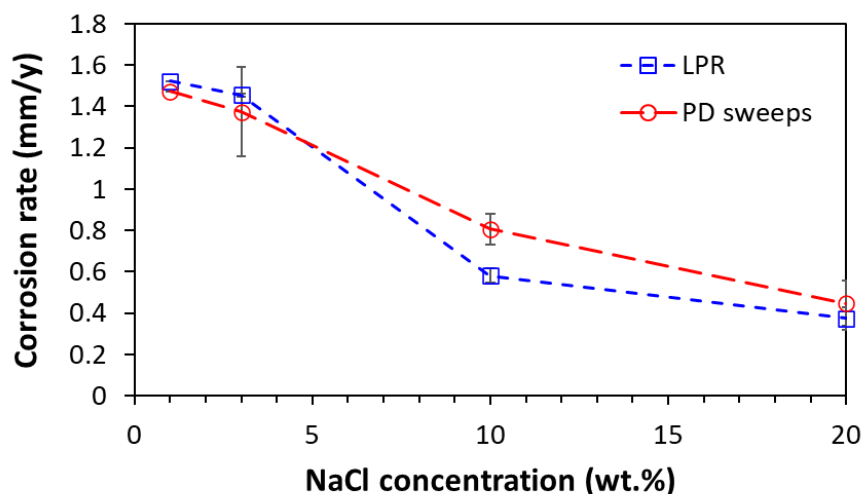


Figure 11. Variations in the corrosion rate of carbon steel X65 RDE vs. NaCl concentration in CO₂ saturated solution at 10°C, 1 bar total pressure, pH 3, and rotational speed of 2000 rpm.

Both techniques show that the corrosion rates decreased with increasing NaCl concentration. As discussed earlier, the decrease in the corrosion rate with the addition of NaCl concentration from 1 wt.% to 20 wt.% was due to deceleration in both anodic and cathodic charge transfer reactions.

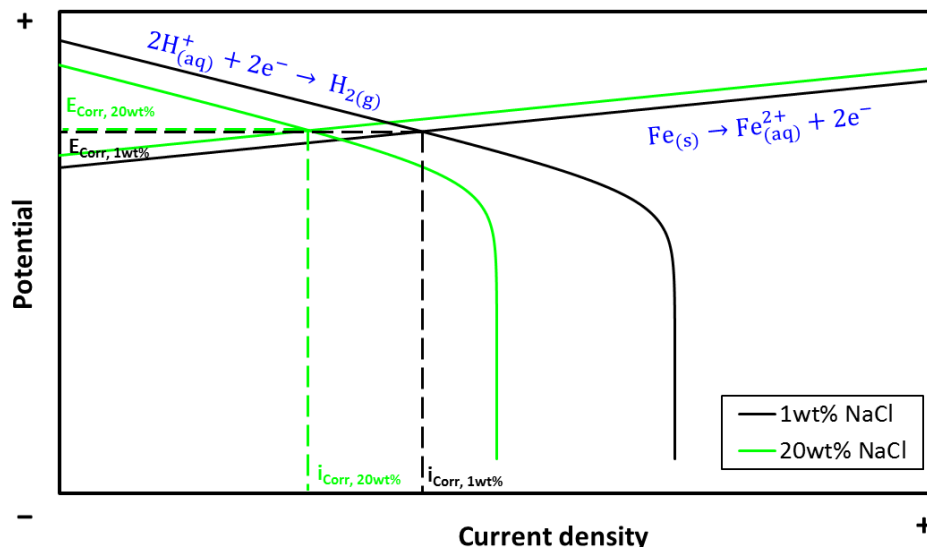


Figure 12. The Evans diagram for the effect of NaCl concentration on uniform CO₂ corrosion of X65 RDE at 10°C, ~1 bar CO₂, pH 3, and 2000 rpm rotational speed. E_{Corr} is the corrosion potential (OPC) and i_{Corr} is the corrosion current density.

Evans diagram

Figure 12 illustrates the Evans diagram for the effect of NaCl concentration on uniform CO₂ corrosion of carbon steel in acidic media, based on the observations in this study. The Evans diagram is obtained by fitting the PD sweeps with the Tafel lines discussed earlier. When NaCl concentration is increased from 1 wt.% to 20 wt.%, the corrosion potential remains almost unchanged, while the corrosion current density decreases, due to retardation of both anodic and cathodic charge transfer reactions. Increasing NaCl concentration also decreases the limiting current density because of a decrease in the concentration of electroactive species and their transfer rate to the electrode surface. The decrease in the limiting current density has almost no effect on the corrosion rate. Therefore, the uniform CO₂ corrosion process is under charge transfer control at these experimental conditions.

CONCLUSIONS

The effect of salt concentration was investigated on uniform CO₂ corrosion of X65 carbon steel by conducting electrochemical experiments with an RDE setup at a rotation rate of 2000 rpm in CO₂-saturated solutions at 10°C, 1 bar total pressure, and pH 3. The following are major conclusions found in this study, when NaCl concentration was increased from 1 wt.% to 20 wt.%:

1. Surface analysis indicated that the CO₂ corrosion process was uniform and no corrosion layer formed on the steel surface.
2. The uniform CO₂ corrosion rate decreased with increasing NaCl concentration.
3. The potentiodynamic polarization sweeps showed that both cathodic (H⁺ reduction) and anodic (iron dissolution) charge transfer reactions were retarded.
4. The cathodic limiting current density decreased due to a reduction in the rate of mass transfer of electroactive species to the surface.
5. NaCl concentration mostly influenced the rate of mass transfer of species to the surface by changing the diffusion coefficient of electroactive species and dissociation equilibria (activity coefficients).
6. Salt concentration did not change the mechanisms of cathodic and anodic reactions.
7. The CO₂ corrosion process was under charge transfer control.

ACKNOWLEDGEMENTS

The authors are greatly thankful to the following companies for their financial support: Anadarko, Baker Hughes, BP, Chevron, Clariant Corporation, ConocoPhillips, DNV GL, ExxonMobil, M-I SWACO (Schlumberger), Multi-Chem (Halliburton), Occidental Oil Company, Pioneer Natural Resources, Saudi Aramco, Shell Global Solutions, SINOPEC (China Petroleum), and TOTAL.

REFERENCES

1. Igunnu, E. T. & Chen, G. Z. Produced water treatment technologies. *Int. J. Low-Carbon Technol.* 9, 157–177 (2014).
2. Breit, G. N. USGS Produced Waters Database. (2002).
3. Fang, H. Low temperature and high salt concentration effects on general CO₂ corrosion for carbon steel. (Ohio University, 2006).
4. Fang, H., Nescic, S., Brown, B. & Wang, S. General CO₂ corrosion in high salinity brines. in No. 06372 (NACE International CORROSION Conference, 2006).
5. Madani Sani, F., Brown, B., Belarbi, Z. & Nescic, S. An experimental investigation on the effect of salt concentration on uniform CO₂ corrosion. in CORROSION Paper No. 13026 (NACE International, 2019).
6. Eliyan, F. F., Mohammadi, F. & Alfantazi, A. An electrochemical investigation on the effect of the chloride content on CO₂ corrosion of API-X100 steel. *Corros. Sci.* 64, 37–43 (2012).
7. Eliyan, F. & Alfantazi, A. Electrochemical investigations on the corrosion behavior and corrosion natural inhibition of API-X100 pipeline steel in acetic acid and chloride-containing CO₂-saturated media. *J. Appl. Electrochem.* 42, 233–248 (2012).
8. Liu, Q. Y., Mao, L. J. & Zhou, S. W. Effects of chloride content on CO₂ corrosion of carbon steel in simulated oil and gas well environments. *Corros. Sci.* 84, 165–171 (2014).
9. Zeng, Z., Lillard, R. S. & Cong, H. Effect of Salt Concentration on the Corrosion Behavior of Carbon Steel in CO₂ Environment. *CORROSION* 72, 805–823 (2016).
10. Han, J., Carey, J. W. & Zhang, J. Effect of sodium chloride on corrosion of mild steel in CO₂-saturated brines. *J. Appl. Electrochem.* 41, 741–749 (2011).
11. Opekar, F. & Beran, P. Rotating disk electrodes. *J. Electroanal. Chem. Interfacial Electrochem.* 69, 1–105 (1976).
12. Madani Sani, F., Afshar, A. & Mohammadi, M. Evaluation of the simultaneous effects of sulfate reducing bacteria, soil type and moisture content on corrosion behavior of buried carbon steel API 5L X65. *Int. J. Electrochem. Sci.* 11, 3887–3907 (2016).
13. Rogers, P. S. Z. & Pitzer, K. S. Volumetric Properties of Aqueous Sodium Chloride Solutions. *J. Phys. Chem. Ref. Data* 11, 15–81 (1982).
14. Nescic, S., Postlethwaite, J. & Olsen, S. An electrochemical model for prediction of corrosion of mild steel in aqueous carbon dioxide solutions. *CORROSION* 52, 280–294 (1996).
15. Hinds, G., Cooling, P., Wain, A., Zhou, S. & Turnbull, A. Technical Note: Measurement of pH in Concentrated Brines. *CORROSION* 65, 635–638 (2009).
16. Bockris, J. O., Drazic, D. & Despic, A. R. The electrode kinetics of the deposition and dissolution of iron. *Electrochimica Acta* 4, 325–361 (1961).
17. Bockris, J. O., McBreen, J. & Nanis, L. The Hydrogen Evolution Kinetics and Hydrogen Entry into a-iron. *J. Electrochem. Soc.* 112, 1025–1031 (1965).
18. Kahyarian, A. Mechanism and Prediction of Mild Steel Corrosion in Aqueous Solutions Containing Carboxylic Acids, Carbon Dioxide, and Hydrogen Sulfide. (Ohio University, 2018).
19. Chin, R. J. & Nobe, K. Electrodissolution Kinetics of Iron in Chloride Solutions III . Acidic Solutions. *J. Electrochem. Soc.* 119, 1457–1461 (1972).
20. McCafferty, E. & Hackerman, N. Kinetics of Iron Corrosion in Concentrated Acidic Chloride Solutions. *J. Electrochem. Soc.* 119, 999–1009 (1972).

21. Lorenz, W. J. & Mansfeld, F. Determination of corrosion rates by electrochemical DC and AC methods. *Corros. Sci.* 21, 647–672 (1981).
22. Burstein, G. T. & Davies, D. H. The effects of anions on the behaviour of scratched iron electrodes in aqueous solutions - ScienceDirect. *Corros. Sci.* 20, 1143–1155 (1980).
23. Duan, Z., Sun, R., Liu, R. & Zhu, C. Accurate Thermodynamic Model for the Calculation of H₂S Solubility in Pure Water and Brines. *Energy Fuels* 21, 2056–2065 (2007).
24. Pitzer, K. S. Thermodynamics of electrolytes. I. Theoretical basis and general equations. *J. Phys. Chem.* 77, 268–277 (1973).
25. Wang, P., Springer, A. & Young, R. D. Modeling phase equilibria and speciation in mixed-solvent electrolyte systems. *Fluid Phase Equilibria* 222–223, 11–17 (2004).
26. Darwish, N. A., Hilbert, F., Lorenz, W. J. & Rosswag, H. The influence of chloride ions on the kinetics of iron dissolution. *Electrochimica Acta* 18, 421–425 (1973).
27. Lorenz, W. J. Der einfluss von halogenidionen auf die anodische auflösung des eisens. *Corros. Sci.* 5, 121–131 (1965).
28. Cavallaro, L., Felloni, L., Trabanelli, G. & Pulidori, F. The anodic dissolution of iron and the behaviour of some corrosion inhibitors investigated by the potentiodynamic method. *Electrochimica Acta* 9, 485–494 (1964).